Polarizabilities of the nucleon and spin dependent photo-absorption

Martin Schumacher

mschuma3@gwdg.de

Zweites Physikalisches Institut der Universität Göttingen, Friedrich-Hund-Platz 1

D-37077 Göttingen, Germany

Abstract

The polarizabilities α (electric), β (magnetic) and γ_π (backward spin) of the nucleon are investigated in terms of the degrees of freedom of the nucleon using recent results for the CGLN amplitudes and resonance couplings $A_{1/2}$ and $A_{3/2}$. The photon excitation strengths of the excited states are given in terms of partial integrated photoabsorption cross sections and resonant contributions of the Gerasimov-Drell-Hearn (GDH) sum rule. As a test of the present predictions, cross section differences $(\sigma_{3/2} - \sigma_{1/2})$ of the excited states are compared with data recently measured at MAMI (Mainz) and ELSA (Bonn). In order to explain differences between proton and neutron, radiative widths of the excited states are compared with nonrelativistic and relativistic predictions based on the $SU(6)$ harmonic oscillator (HO) quark model. A complete list of partial contributions from the s-channel and the t-channel are given for the polarizabilities.

1   Introduction

The present work is a continuation of a systematic series of studies [1–4] on the electromagnetic structure of the nucleon, following experimental work on Compton scattering and a comprehensive review on this topic [5]. These recent investigations have shown [1–4] that a systematic study of all partial resonant and nonresonant photo-excitation processes of the nucleon and of their relevance for the fundamental structure constants of the nucleon as there are the electric polarizability (α), the magnetic polarizability (β) and the backward spin-polarizability (γ_π) is essential for an understanding of the electromagnetic structure of the nucleon. In addition it has been found that the structure of the constituent quarks and their coupling to pseudoscalar and scalar mesons is important for the understanding of the electric and magnetic polarizabilities and of the backward spin-polarizability. The reason is that neutral scalar mesons couple to two photons with parallel planes of linear polarization and, therefore, make sizable t-channel contributions to the electric and magnetic polarizabilities whereas neutral pseudoscalar mesons couple to two photons with perpendicular planes of linear polarization and, therefore, make a sizable t-channel contribution to the backward spin-polarizability. In the course of these studies it has been found desirable to have a better understanding of the level structure of the nucleon and of the cross section components entering into the resonant parts of the polarizabilities. Especially, it had to be clarified whether characteristic differences found between the excited states of the proton and the neutron can be related to the quark-structure of these particles. Since the backward spin-polarizability depends on the helicity dependent photo-absorption cross section, also this cross section was investigated.

This latter part of the work was made possible by recent precise measurements of helicity dependent cross sections carried out at MAMI (Mainz) and ELSA (Bonn) using circularly polarized photons and spin-polarized proton and deuteron targets [6–19]. These studies have led to important data which have been used for a test of the Gerasimov-Drell-Hearn (GDH) sum rule. The GDH sum rule relates the energy-weighted difference $(\sigma_{3/2} - \sigma_{1/2})$ of spin dependent cross sections to the square of the anomalous magnetic moment κ of the nucleon and in this

way makes an important contribution to the studies of the spin-structure of the nucleon. All aspects of the experiment and the interpretation of the data have been nicely reviewed in a recent article [20] (see also [21]).

A further motivation for the present work was provided by the fact that the knowledge of CGLN amplitudes and of the resonance couplings $A_{1/2}$ and $A_{3/2}$ has been improved to a large extent due to recent very precise MAID (Mainz) analyses of photo-absorption data in terms of CGLN amplitudes [22] (see also [23]). This made it possible to considerably improve on the prediction of spin and multipolarity dependent photo-absorption cross sections and, therefore, also on the polarizabilities of the nucleon.

2 Outline of the method

Walker [24, 25] writes the integral cross sections for pion photoproduction in terms of helicity "elements" (or amplitudes) $A_{l\pm}$ and $B_{l\pm}$, given in the form

$$\sigma_T = \frac{1}{2}(\sigma_{1/2} + \sigma_{3/2}),$$

$$\sigma_{1/2} = \frac{8\pi q}{k} \sum_{l=0}^{\infty} (l+1)(|A_{l+}|^2 + |A_{(l+1)-}|^2),$$

$$\sigma_{3/2} = \frac{8\pi q}{k} \sum_{l=0}^{\infty} \frac{1}{4}[l(l+1)(l+2)](|B_{l+}|^2 + |B_{(l+1)-}|^2), \tag{1}$$

where the subscript notation of the A's and B's is the same as that of the CGLN; e.g. $B_{l\pm}$ refers to a state with pion orbital angular momentum l and total angular momentum $J = l \pm \frac{1}{2}$. The A's and B's differ in the absolute values of the helicities $\Lambda = |\lambda|$ of the initial states given by $\lambda = \lambda_\gamma - \lambda_p$, where λ_γ is the helicity of the incident photon and λ_p the helicity of the nucleon in the initial state. For the A's the helicity is $\Lambda = 1/2$ for the B's $\Lambda = 3/2$. The quantity q is the 3-momentum of the pion and k the 3-momentum of the photon in the c.m. system.

Walker [24] finds the following relations between the helicity elements and the CGLN multipole coefficients:

$$A_{k+} = \frac{1}{2}[(k+2)E_{k+} + kM_{k+}], \quad B_{k+} = E_{k+} - M_{k+},$$

$$A_{(k+1)-} = \frac{1}{2}[-kE_{(k+1)-} + (k+2)M_{(k+1)-}],$$

$$B_{(k+1)-} = E_{(k+1)-} + M_{(k+1)-}. \tag{2}$$

From isospin consideration it has been derived that the amplitudes for meson photoproduction A are composed of $A^{(1/2)}$ and $A^{(3/2)}$, referring to final states of definite isospin ($\frac{1}{2}$) or ($\frac{3}{2}$). Furthermore, there is an amplitude $A^{(0)}$ corresponding to the isoscalar transition. This latter amplitude makes a contribution to $I = 1/2$ only. Therefore, the amplitudes

$$_pA^{(1/2)} = A^{(0)} + \frac{1}{3}A^{(1/2)}$$

$$_nA^{(1/2)} = A^{(0)} - \frac{1}{3}A^{(1/2)} \tag{3}$$

may be introduced. Furthermore, with

$$A^{(+)} = \frac{1}{3}(A^{(1/2)} + 2A^{(3/2)}),$$

$$A^{(-)} = \frac{1}{3}(A^{(1/2)} - A^{(3/2)}), \tag{4}$$

2

the physical amplitudes may be expressed by the isospin combinations (see, e.g., [26, 27])

$$A(\gamma p \to n\pi^+) = \sqrt{2}(A^{(-)} + A^{(0)}) = \sqrt{2}\left({}_pA^{(1/2)} - \frac{1}{3}A^{(3/2)}\right), \tag{5}$$

$$A(\gamma p \to p\pi^0) = A^{(+)} + A^{(0)} = {}_p A^{(1/2)} + \frac{2}{3}A^{(3/2)}, \tag{6}$$

$$A(\gamma n \to p\pi^-) = -\sqrt{2}(A^{(-)} - A^{(0)}) = \sqrt{2}\left({}_nA^{(1/2)} + \frac{1}{3}A^{(3/2)}\right), \tag{7}$$

$$A(\gamma n \to n\pi^0) = A^{(+)} - A^{(0)} = -{}_nA^{(1/2)} + \frac{2}{3}A^{(3/2)}. \tag{8}$$

From these equations we arrive at the isospin decompositions

$$|A|^2(\text{proton}) = |A(\gamma p \to n\pi^+)|^2 + |A(\gamma p \to p\pi^0)|^2 = 3|_pA^{(1/2)}|^2 + \frac{2}{3}|A^{(3/2)}|^2, \tag{9}$$

$$|A|^2(\text{neutron}) = |A(\gamma n \to p\pi^-)|^2 + |A(\gamma n \to n\pi^0)|^2 = 3|_nA^{(1/2)}|^2 + \frac{2}{3}|A^{(3/2)}|^2. \tag{10}$$

Making use of (9) and (10) we arrive at the helicity and isospin dependent cross sections for the most important multipoles. These relations are valid for the 1π channel only.

$$\sigma_{1/2}^{(1\pi)}(0+) = \frac{8\pi q}{k}\left[3\left|_{(p.n)}E_{0+}^{(1/2)}\right|^2 + \frac{2}{3}\left|E_{0+}^{(3/2)}\right|^2\right], \tag{11}$$

$$\sigma_{3/2}^{(1\pi)}(0+) = 0, \tag{12}$$

$$\sigma_{1/2}^{(1\pi)}(1-) = \frac{8\pi q}{k}\left[3\left|_{(p.n)}M_{1-}^{(1/2)}\right|^2 + \frac{2}{3}\left|M_{1-}^{(3/2)}\right|^2\right], \tag{13}$$

$$\sigma_{3/2}^{(1\pi)}(1-) = 0, \tag{14}$$

$$\sigma_{1/2}^{(1\pi)}(1+) = \frac{8\pi q}{k}\frac{1}{2}\left[3\left|3_{(p.n)}E_{1+}^{(1/2)} + _{(p.n)}M_{1+}^{(1/2)}\right|^2 + \frac{2}{3}\left|3E_{1+}^{(3/2)} + M_{1+}^{(3/2)}\right|^2\right], \tag{15}$$

$$\sigma_{3/2}^{(1\pi)}(1+) = \frac{8\pi q}{k}\frac{3}{2}\left[3\left|_{(p,n)}E_{1+}^{(1/2)} - _{(p.n)}M_{1+}^{(1/2)}\right|^2 + \frac{2}{3}\left|E_{1+}^{(3/2)} - M_{1+}^{(3/2)}\right|^2\right], \tag{16}$$

$$\sigma_{1/2}^{(1\pi)}(2-) = \frac{8\pi q}{k}\frac{1}{2}\left[3\left|-_{(p.n)}E_{2-}^{(1/2)} + 3_{(p.n)}M_{2-}^{(1/2)}\right|^2 + \frac{2}{3}\left|-E_{2-}^{(3/2)} + 3M_{2-}^{(3/2)}\right|^2\right], \tag{17}$$

$$\sigma_{3/2}^{(1\pi)}(2-) = \frac{8\pi q}{k}\frac{3}{2}\left[3\left|_{(p,n)}E_{2-}^{(1/2)} + _{(p.n)}M_{2-}^{(1/2)}\right|^2 + \frac{2}{3}\left|E_{2-}^{(3/2)} + M_{2-}^{(3/2)}\right|^2\right], \tag{18}$$

$$\sigma_{1/2}^{(1\pi)}(2+) = \frac{8\pi q}{k}3\left[3\left|2_{(p.n)}E_{2+}^{(1/2)} + _{(p.n)}M_{2+}^{(1/2)}\right|^2 + \frac{2}{3}\left|2E_{2+}^{(3/2)} + M_{2+}^{(3/2)}\right|^2\right], \tag{19}$$

$$\sigma_{3/2}^{(1\pi)}(2+) = \frac{8\pi q}{k}6\left[3\left|_{(p,n)}E_{2+}^{(1/2)} - _{(p.n)}M_{2+}^{(1/2)}\right|^2 + \frac{2}{3}\left|E_{2+}^{(3/2)} - M_{2+}^{(3/2)}\right|^2\right], \tag{20}$$

$$\sigma_{1/2}^{(1\pi)}(3-) = \frac{8\pi q}{k}3\left[3\left|-_{(p,n)}E_{3-}^{(1/2)} + 2_{(p.n)}M_{3-}^{(1/2)}\right|^2 + \frac{2}{3}\left|-E_{3-}^{(3/2)} + 2M_{3-}^{(3/2)}\right|^2\right], \tag{21}$$

$$\sigma_{3/2}^{(1\pi)}(3-) = \frac{8\pi q}{k}6\left[3\left|_{(p,n)}E_{3-}^{(1/2)} + _{(p.n)}M_{3-}^{(1/2)}\right|^2 + \frac{2}{3}\left|E_{3-}^{(3/2)} + M_{3-}^{(3/2)}\right|^2\right], \tag{22}$$

$$\sigma_{1/2}^{(1\pi)}(3+) = \frac{8\pi q}{k}\left[3\left|5_{(p.n)}E_{3+}^{(1/2)} + 3_{(p.n)}M_{3+}^{(1/2)}\right|^2 + \frac{2}{3}\left|5E_{3+}^{(3/2)} + 3M_{3+}^{(3/2)}\right|^2\right], \tag{23}$$

$$\sigma_{3/2}^{(1\pi)}(3+) = \frac{8\pi q}{k}15\left[3\left|_{(p,n)}E_{3+}^{(1/2)} - _{(p.n)}M_{3+}^{(1/2)}\right|^2 + \frac{2}{3}\left|E_{3+}^{(3/2)} - M_{3+}^{(3/2)}\right|^2\right]. \tag{24}$$

It is generally assumed [22, 28] that the inelasticity (2π and η) correction is independent of the helicity[1]. This implies that the difference of helicity dependent cross sections ($\sigma_{3/2} - \sigma_{1/2}$) and the total photo-absorption cross section $\sigma_T = \frac{1}{2}(\sigma_{3/2} + \sigma_{1/2})$ are proportional to each other:

$$\sigma_{3/2} - \sigma_{1/2} = A_n \, \frac{1}{2}(\sigma_{3/2} + \sigma_{1/2}) \tag{25}$$

where for non-mixed multipolarity we have $A_n = -2$ for E_{0+} and M_{1-}, $A_n = +1$ for M_{1+} and E_{2-}, $A_n = +2/3$ for M_{2+} and E_{3-}, and $A_n = 1/2$ for M_{3+}. For mixed multipolarity the proportionality constant is given by

$$A_n = \left[\frac{2(\sigma_{3/2} - \sigma_{1/2})}{\sigma_{3/2} + \sigma_{1/2}} \right]_{\text{res.}} \tag{26}$$

and can easily be calculated from the CGLN amplitudes [22] at resonance maximum where only the imaginary parts are of importance. However, thereafter slight corrections are possible because of a slight energy dependence of A_n which may be determined by considering the CGLN amplitudes over the entire resonance or by adjusting to experimental data. The latter procedure will be carried out in subsection 4.2.

The advantage of using Eq. (25) is that the very convenient Walker parameterization [24, 29] of nucleon resonant cross sections derived for $\sigma_T = \frac{1}{2}(\sigma_{3/2} + \sigma_{1/2})$ can also be applied to ($\sigma_{3/2} - \sigma_{1/2}$). For convenience we give the Walker parameterization in the following (see [29] for the presently used definitions and the choice of damping factors):

$$I = I_r \left(\frac{k_r}{k} \right)^2 \frac{W_r^2 \, \Gamma \, \Gamma_\gamma^*}{(W^2 - W_r^2)^2 + W_r^2 \Gamma^2}, \tag{27}$$

$$\Gamma = \Gamma_r \left(\frac{q}{q_r} \right)^{2l+1} \left(\frac{q_r^2 + X^2}{q^2 + X^2} \right)^l, \tag{28}$$

$$\Gamma_\gamma^* = \Gamma_r \left(\frac{k}{k_r} \right)^{2j_\gamma} \left(\frac{k_r^2 + X^2}{k^2 + X^2} \right)^{j_\gamma}, \tag{29}$$

$$s = 2\omega m + m^2, \tag{30}$$

$$\omega = \text{ photon energy in the lab. system,} \tag{31}$$

$$m = \text{ nucleon mass ,} \tag{32}$$

$$W^2 = s, \tag{33}$$

$$k = |\mathbf{k}| = \frac{s - m^2}{2\sqrt{s}}, \tag{34}$$

$$|\mathbf{k}| = \text{photon 3-momentum in the c.m. system,} \tag{35}$$

$$q = |\mathbf{q}| = \sqrt{E_\pi^2 - m_\pi^2}; \quad E_\pi = \frac{s - m^2 + m_\pi^2}{2\sqrt{s}}, \tag{36}$$

$$|\mathbf{q}| = \pi \text{ 3-momentum in the c.m. system,} \tag{37}$$

$$j_\gamma, \text{ multipole angular momentum of the photon,} \tag{38}$$

$$l, \text{ single } \pi \text{ angular momentum.} \tag{39}$$

The quantities I_r, Γ_r, k_r, q_r are the peak cross section, the width of the resonance, the photon 3-momentum and pion 3-momentum at resonance in the c.m. system. The damping constants X are $X = 160$ MeV for the $P_{33}(1232)$-resonance and $X = 350$ MeV else. The peak cross-section

---

[1]The same branching correction Γ/Γ_π is used to relate $A_{1/2}$ and $A_{3/2}$ to the CGLN amplitudes.

I_r introduced in (27) is given by[2]

$$I_r = 2\,\pi\,\frac{1}{k_r^2}\frac{2\,J+1}{2\,J_0+1}\frac{\Gamma_\gamma}{\Gamma}, \tag{40}$$

where J and J_0 are the spins of the excited states and the ground state, respectively, Γ_γ the photon width and Γ the total width of the resonance. The photon width Γ_γ may be expressed through the resonance couplings $A_{1/2}$ and $A_{3/2}$ by the relation [30]

$$\Gamma_\gamma = \frac{k_r^2}{\pi}\frac{2M_N}{(2J+1)M_R}[|A_{1/2}|^2 + |A_{3/2}|^2], \tag{41}$$

where M_N and M_R are the nucleon and resonant masses. Combining (40) and (41) we arrive at

$$I_r = \frac{2M_N}{M_R\Gamma}[|A_{1/2}|^2 + |A_{3/2}|^2]. \tag{42}$$

One advantage of the present approach over other approaches based on the CGLN amplitudes is that the quantity I_r defined in (42) contains the branching correction Γ/Γ_π.

It is of interest to compare the present approach with previous approaches. At the resonance energy the partial cross sections given in (11) – (24) are related to the resonance couplings introduced by Arndt et al. [31] through the relations (see Eq. (42))

$$\sigma_{1/2,\,3/2}^{(1\pi)}(l\pm)(\Gamma/\Gamma_\pi) = \frac{4\,M_N}{M_R\,\Gamma}|A_{l\pm}^{1/2,\,3/2}|^2 \tag{43}$$

where Γ_π is the πN elastic width. These resonance couplings are related to the electric and magnetic multipoles via the relations

$$A_{l+}^{1/2} = -\frac{1}{2}[(l+2)\,\overline{E}_{l+} + l\,\overline{M}_{l+}], \tag{44}$$

$$A_{l+}^{3/2} = \frac{1}{2}\sqrt{l(l+2)}[\overline{E}_{l+} - \overline{M}_{l+}], \tag{45}$$

$$A_{(l+1)-}^{1/2} = -\frac{1}{2}[l\,\overline{E}_{(l+1)-} - (l+2)\overline{M}_{(l+1)-}], \tag{46}$$

$$A_{(l+1)-}^{3/2} = -\frac{1}{2}\sqrt{l(l+2)}[\overline{E}_{(l+1)-} + \overline{M}_{(l+1)-}], \tag{47}$$

where the above barred multipoles are related to the CGLN (E, M) multipoles at resonance energy W_r through the relations

$$(\overline{E},\overline{M}) = C\left[\frac{(2j+1)\pi q_r W_r \Gamma_r^2}{k_r M_N \Gamma_\pi}\right]^{1/2}(E, M). \tag{48}$$

The factor C in Eq. (48) is $\sqrt{2/3}$ for isospin $\frac{3}{2}$ and $-\sqrt{3}$ for isospin $\frac{1}{2}$. It is easy to see that the approach outlined in Eqs. (43) – (48) leads to the same result as the relations (11) – (24) at the resonance energy W_r.

---

[2] Please note that the quantity Γ_γ^* in Eq. (29) has a different definition as the quantity Γ_γ in the following Eqs. (40) and (41).

3 The level structure of the nucleon

A comprehensive outline of the structure of baryons in terms of quark models has recently been given by the Particle Data Group [30]. Therefore, in this section we may restrict the discussion to those aspects which are of special interest for the present investigation and not covered in that article.

It has been successful [30, 32–43] to classify nucleon resonances in terms of the spin-flavor SU(6) harmonic oscillator (HO) model. Empirically we know that the ground state of the harmonic oscillator ($N = 0$) is a $(\mathbf{56}, L^P = 0^+)$ super-multiplet state. The first excited state ($N = 1$) consists of the $(\mathbf{70}, 1^-)$ super multiplet only. The second excited state ($N = 2$) consists of the $(\mathbf{56}, 0^+)$, $(\mathbf{56}, 2^+)$, $(\mathbf{70}, 0^+)$ and $(\mathbf{70}, 2^+)$ super multiplets of which $(\mathbf{70}, 0^+)$ and $(\mathbf{70}, 2^+)$ are barely seen experimentally. Reasons for the preference of the $(\mathbf{56}, 0^+)$, $(\mathbf{56}, 2^+)$ super multiplets have been discussed e.g. in [33, 34, 37, 40].

3.1 Empirical level scheme based on the $SU(6)$-HO quark model

The excitation spectrum of the nucleon constructed on the basis of the classification scheme outlined above is shown in Table 1 and in the level scheme of Figure A1 given in the appendix. Column 1 of Table 1 shows the oscillator quantum number N, the angular momentum L of the HO subshell and the dimension of the corresponding super multiplet. Column 2 shows the spectroscopic configuration

$$^{2S+1}L_J^{(I)} \tag{49}$$

and the (SU(3),SU(2)) subgroup dimensions of states possible for the given harmonic oscillator subshell. In (49) S, L, J and I are the spin, orbital angular momentum, total angular momentum and isospin of the state, where $L = 0, 1, 2, \cdots$ has been represented by $S, P, D. \cdots$, respectively. Within the subgroups the order of levels is according to the size of the total angular momentum J. Column 3 shows nucleon resonances and the corresponding electromagnetic and CGLN multipoles which have to be attributed to the spectroscopic configurations of column 2. All the states expected in the first three oscillator shells have been included, except for the $N = 2$ $(\mathbf{70}, 0^+)$ resonances $P_{11}(1710)$ which has the $***$ status. The $***$ $D_{35}(1930)$ resonance which energetically fits into the third oscillator shell is a member of the fourth oscillator shell because of its parity. Column 4 shows the integrated photo-absorption cross sections ($I_{int.}$) corresponding to the resonances and are given for the proton (p) and the neutron (n). These numbers are described in more detail in appendix B.

In the second oscillator shell we find 7 levels in total. They belong to the subgroups $(8, 2)$ or $(I = 1/2, S = 1/2)$, $(8, 4)$ or $(I = 1/2, S = 3/2)$ and $(10, 4)$ or $(I = 3/2, S = 3/2)$. The two states $D_{13}(1520)$ and $S_{11}(1535)$ form the second resonance region of the nucleon photo-excitation spectrum whereas the $D_{33}(1700)$ state makes a contribution to the third resonance region in addition to the $F_{15}(1680)$, stemming from the third oscillator shell. The other states contain less strength and do not lead to pronounced structures in the nucleon photo-excitation spectrum. There are 8 nucleon levels of the third oscillator shell. The $N = 2$ $(\mathbf{56}, 0^+)$ state contains the Roper resonance $P_{11}(1440)$ and the Δ resonance state $P_{33}(1600)$ build upon the Roper resonance. These two states do not lead to pronounced structures in the photo-excitation spectrum of the nucleon. In contrast to this the $N = 2$ $(\mathbf{56}, 2^+)$ state contains two states, $F_{15}(1680)$ and the $F_{37}(1950)$, which are the most prominent members of the third and fourth resonance regions of the nucleon photo-excitation spectrum.

Table 1 reveals that within the subgroups corresponding to a given set of quantum numbers (N, L, I, S) the fully stretched member, i.e. the one with the largest J, in general contains

Table 1: Nucleon resonant states and meson photoproduction for the first three oscillator shells. The integrated cross sections in column 4 ($I_{int.}$) are based on the resonance couplings $A_{1/2}$ and $A_{3/2}$ of the proton (p) and the neutron (n). Within the subgroups the states are ordered with respect to the size of the total angular momentum J.

	$^{2S+1}L_J^{(I)}$		$I_{int.}$ $[10^3\,\mu\text{b MeV}]$	
$N=0,\ L=0$	$^2S_{1/2}^{(1/2)}\,(8,2)$	$P_{11}(939)$	p	n
$(\mathbf{56},0^+)$	$^4S_{3/2}^{(3/2)}\,(10,4)$	$M1,(E2) \to P_{33}(1232) \to M_{1+}^{(3/2)},(E_{1+}^{(3/2)})$	80.0	80.0
$N=2,\ L=0$	$^2S_{1/2}^{(1/2)}\,(8,2)$	$M1 \to P_{11}(1440) \to {}_{p,n}M_{1-}^{(1/2)}$	3.4	1.3
$(\mathbf{56},0^+)$	$^4S_{3/2}^{(3/2)}\,(10,4)$	$M1,(E2) \to P_{33}(1600) \to M_{1+}^{(3/2)},(E_{1+}^{(3/2)})$	0.7	0.7
$N=1,\ L=1$	$^2P_{1/2}^{(1/2)}\,(8,2)$	$E1 \to S_{11}(1535) \to {}_{p,n}E_{0+}^{(1/2)}$	8.8	2.4
$(\mathbf{70},1^-)$	$^2P_{3/2}^{(1/2)}\,(8,2)$	$E1,(M2) \to D_{13}(1520) \to {}_{p,n}E_{2-}^{(1/2)},({}_{p,n}M_{2-}^{(1/2)})$	34.6	27.9
$N=1,\ L=1$	$^2P_{1/2}^{(3/2)}\,(10,2)$	$E1 \to S_{31}(1620) \to E_{0+}^{(3/2)}$	0.9	0.9
$(\mathbf{70},1^-)$	$^2P_{3/2}^{(3/2)}\,(10,2)$	$E1,(M2) \to D_{33}(1700) \to E_{2-}^{(3/2)},(M_{2-}^{(3/2)})$	18.0	18.0
$N=1,\ L=1$	$^4P_{1/2}^{(1/2)}\,(8,4)$	$E1 \to S_{11}(1650) \to {}_{p,n}E_{0+}^{(1/2)}$	3.1	0.2
$(\mathbf{70},1^-)$	$^4P_{3/2}^{(1/2)}\,(8,4)$	$E1,(M2) \to D_{13}(1700) \to {}_{p,n}E_{2-}^{(1/2)},({}_{p,n}M_{2-}^{(1/2)})$	0.4	0.1
	$^4P_{5/2}^{(1/2)}\,(8,4)$	$M2,(E3) \to D_{15}(1675) \to {}_{p,n}M_{2+}^{(1/2)},({}_{p,n}E_{2+}^{(1/2)})$	0.7	6.2
$N=2,\ L=2$	$^2D_{3/2}^{(1/2)}\,(8,2)$	$M1,(E2) \to P_{13}(1720) \to {}_{p,n}M_{1+}^{(1/2)},({}_{p,n}E_{1+}^{(1/2)})$	0.8	1.0
$(\mathbf{56},2^+)$	$^2D_{5/2}^{(1/2)}\,(8,2)$	$E2,(M3) \to F_{15}(1680) \to {}_{p,n}E_{3-}^{(1/2)},({}_{p,n}M_{3-}^{(1/2)})$	19.9	2.2
$N=2,\ L=2$	$^4D_{1/2}^{(3/2)}\,(10,4)$	$M1 \to P_{31}(1910) \to M_{1-}^{(3/2)}$	<0.1	<0.1
$(\mathbf{56},2^+)$	$^4D_{3/2}^{(3/2)}\,(10,4)$	$M1,(E2) \to P_{33}(1920) \to M_{1+}^{(3/2)},(E_{1+}^{(3/2)})$	2.3	2.3
	$^4D_{5/2}^{(3/2)}\,(10,4)$	$E2,(M3) \to F_{35}(1905) \to E_{3-}^{(3/2)},(M_{3-}^{(3/2)})$	2.7	2.7
	$^4D_{7/2}^{(3/2)}\,(10,4)$	$M3,(E4) \to F_{37}(1950) \to M_{3+}^{(3/2)},(E_{3+}^{(3/2)})$	15.8	15.8

the largest photo-excitation strength. States with $I = 3/2$ have the same photo-excitation strength for the proton and the neutron because the transition from the ground state to the excited state is possible through an isovector transition only. On the other hand, for states with $I = 1/2$ the excitation is possible via isoscalar and isovector transitions and, therefore, the proton and neutron may contain different photo-excitation strengths. As a general rule we find that for the proton the photo-excitation strength is larger than for the neutron with the remarkable exception of the $D_{15}(1675)$ resonance where the neutron contains a ten times larger photon excitation strength than the proton. This latter finding is in agreement with the Moorhouse selection rule [32, 33] according to which in the quark model the photon width $\Gamma_\gamma(D_{15}^+(1675) \to p\gamma) = 0$ whereas $\Gamma_\gamma(D_{15}^0(1675) \to n\gamma) \neq 0$. Further information concerning the photon widths of the levels of the nucleon obtained from the quark model are given in the following subsection.

3.2 Radiative widths Γ_γ predicted in the quark model

Radiative widths Γ_γ of nucleon resonances in the nonrelativistic $SU(6)$-HO model have been derived by Faiman and Hendry [33]. In these calculations the oscillator spring constant α^2 and the constituent-quark g-factor are treated as adjustable parameters. In the same model the resonance couplings $A_{1/2}$ and $A_{3/2}$ are calculated by Copley et al. [35]. In this work the g-factor g=1 is used but again the oscillator spring constant is teated as an adjustable parameter. The number given in that work, *viz.* $\alpha^2 = 0.17$ GeV^2, together with $g = 1$ are used in general in later work. A complete list of results for the resonance couplings $A_{1/2}$ and $A_{3/2}$ are calculated by Koniuk and Isgur [38].

The general structure of the expression describing the radiative width in the nonrelativistic $SU(6)$-HO quark model is given by

$$\Gamma_\gamma = a\, k^3 (k^2/\alpha^2)^N [g^2 + b(\alpha^2/k^2)g + c(\alpha^4/k^4)]B \qquad (50)$$

where k is the photon 3-momentum in the c.m. system, N the oscillator quantum number

Table 2: Experimental nucleon radiative widths for the first three oscillator shells compared with $SU(6)$-HO model predictions. (a) nonrelativistic quark model [33, 35, 38], (b) relativized quark model [41], (c) relativized quark model [43].

	proton				Γ_γ [MeV]	neutron			
	experiment	th.(a)	th. (b)	th.(c)		experiment	th.(a)	th. (b)	th.(c)
$P_{33}(1232)$	0.69 ± 0.02	0.33	0.41	0.37		0.69 ± 0.02	0.33	0.41	0.37
$P_{11}(1440)$	0.15 ± 0.02	0.02	0.004	0.0006		0.06 ± 0.03	0.009	0.004	0.0013
$P_{33}(1600)$	$0.02^{+0.05}_{-0.01}$	0.03	0.02	0.09		$0.02^{+0.05}_{-0.01}$	0.03	0.02	0.09
$S_{11}(1535)$	0.36 ± 0.16	1.3	1.2	0.26		$0.09^{+0.14}_{-0.08}$	0.7	0.5	0.18
$D_{13}(1520)$	0.61 ± 0.04	0.35	0.40	0.39		0.49 ± 0.07	0.38	0.51	0.31
$S_{31}(1620)$	0.04 ± 0.03	0.2	0.6	0.4		0.04 ± 0.03	0.2	0.6	0.4
$D_{33}(1700)$	0.55 ± 0.15	0.58	0.33	0.35		0.55 ± 0.15	0.58	0.33	0.35
$S_{11}(1650)$	0.16 ± 0.10	0.0	0.04	0.16		$0.013^{+0.060}_{-0.010}$	0.04	0.006	0.07
$D_{13}(1700)$	$0.010^{+0.015}_{-0.010}$	0.0	0.09	0.03		$0.03^{+0.09}_{-0.03}$	0.13	0.04	0.04
$D_{15}(1675)$	0.011 ± 0.008	0.0	0.0	0.0003		0.10 ± 0.04	0.08	0.13	0.08
$P_{13}(1720)$	$0.02^{+0.09}_{-0.02}$	0.4	0.3	0.03		$0.03^{+0.09}_{-0.02}$	0.03	0.009	0.004
$F_{15}(1680)$	0.36 ± 0.06	0.11	0.19	0.09		0.04 ± 0.02	0.02	0.03	0.018
$P_{31}(1910)$	$0.001^{+0.007}_{-0.001}$	0.03	0.03	0.005		$0.001^{+0.007}_{-0.001}$	0.03	0.03	0.005
$P_{33}(1920)$	0.09 ± 0.06	0.07	0.04	0.015		0.09 ± 0.06	0.07	0.04	0.015
$F_{35}(1905)$	0.07 ± 0.05	0.09	0.08	0.02		0.07 ± 0.05	0.09	0.08	0.02
$F_{37}(1950)$	0.33 ± 0.06	0.07	0.14	0.06		0.33 ± 0.06	0.07	0.14	0.06

and B a factor containing the quark level magnetic moment $\mu = \mu_p$, the factor $\exp(-k^2/(3\alpha^2))$ characterizing the harmonic oscillator and a kinematical factor. The specific $SU(6)$ spin-flavor properties of the nuclear levels are contained in the quantities a, b and c which are rational numbers and may be found in [33] or derived from the results given in [35] and [38]. As far as

the quantities a are nonzero we find that for $I = 1/2$ these number are smaller for the neutron than for the proton. The proton-neutron ratio of the quantity a is 9/4 for P_{11}, P_{13} and F_{15} states, and 9 for S_{11} and D_{13} states. This is in qualitative agreement with the observation that the integrated cross section given in Table 1 are in general smaller for the neutron than for the proton. This means that qualitatively the difference in photo-excitation strength of proton and neutron may be understood in terms of the $SU(6)$-HO quark model. In some cases as e.g. for the $D_{13}(1520)$ state the different factors a for the proton and the neutron are compensated by the expression in square brackets so that the photo-excitation strengths are almost the same for the two nucleons.

It was pointed out in other works (see e.g. [36, 39, 41, 43] and references therein) that the nonrelativistic version of the SU(6)-HO model should be supplemented by relativistic corrections. Of these we give special attention to the two latest calculation carried out by Close and Li [41] and by Capstick [43]. Numerical results for the photon widths are given in Table 2. The experimental data are calculated from the resonance couplings given in Table B1 and B2. The predictions (a) are based on the nonrelativistic $SU(6)$-HO model with the parameter $\alpha^2 = 0.17$ GeV^2 and $g = 1$ as derived by Copley et al [35] and also used in later work. The predictions (b) have been obtained [41] by supplementing the nonrelativistic results by spin-orbit terms. The predictions (c) have been obtained in a quark model [43] where an electromagnetic transition operator is used containing relativistic corrections, and relativized-quark-model wave functions.

A special feature is that in the nonrelativistic $SU(6)$-HO quark model the proton radiative widths of the $S_{11}(1650)$, $D_{13}(1700)$ and $D_{15}(1675)$ are equal to zero. For the $D_{15}(1675)$ state this feature is known as the Moorhouse selection rule [32] whereas for the $S_{11}(1650)$ and $D_{13}(1700)$ states two other states, viz. $S_{11}(1535)$ and $D_{13}(1520)$ with the same quantum numbers exist so that the physical states are linear combinations. The corresponding expressions are given in [33]. Mixing angles are given in [30]. The relativized predictions (b) and (c) in general are in better agreement with the experimental data than the nonrelativistic predictions (a) though some apparent drawbacks are visible in all three cases. As a summary we may state, that qualitatively the nonrelativistic and the relativistic $SU(6)$-HO quark models explain many features of the radiative widths. Especially it is explained that for $I = 1/2$ the radiative widths of the neutron are in general smaller than those of the proton, except for the effects of the Moorhouse selection rule.

It should be mentioned that very recently progress has been made by developing a hyper-central constituent quark model with a meson cloud [44]. The predicted resonance couplings $A_{3/2}$ and $A_{1/2}$ for the $P_{33}(1232)$ resonance are in a better agreement with the experimental values with the pion cloud than without the pion cloud. Further results are expected for the $S_{11}(1535)$ and the $D_{13}(1520)$ resonances.

4   The Gerasimov-Drell-Hearn sum rule

Using dispersion theory as outlined in [45] and [5] we arrive at

$$\frac{1}{\omega}\operatorname{Re} g_0(\omega) = \operatorname{Re} g(\omega) = -\frac{\alpha_e}{2}\left(\frac{\kappa}{m}\right)^2 + \frac{\omega^2}{4\pi^2}\mathcal{P}\int_{\omega_0}^{\infty}\frac{d\omega'}{\omega'}\frac{\Delta\sigma(\omega')}{\omega'^2 - \omega^2}, \tag{51}$$

where $\alpha_e = 1/137.04$ and

$$\Delta\sigma(\omega) = \sigma_{1/2}(\omega) - \sigma_{3/2}(\omega). \tag{52}$$

This leads to

$$\operatorname{Re} g(\infty) = -\frac{\alpha_e}{2}\left(\frac{\kappa}{m}\right)^2 - \frac{1}{4\pi^2}\int_{\omega_0}^{\infty}\frac{d\omega'}{\omega'}\Delta\sigma(\omega'). \tag{53}$$

Table 3: Lines 3–13: Nucleon resonances observed via spin independent or helicity dependent measurements of the photo-absorption cross section of the nucleon. The very weak resonances $P_{33}(1600)$, $S_{31}(1620)$, $D_{13}(1700)$, $P_{13}(1720)$ and $P_{31}(1910)$ have been omitted. The quantity A_n in the second column is the scaling factor of Eq. (25) for the leading multipole, $A_n(\text{proton})$ and $A_n(\text{neutron})$ the corresponding scaling factors obtained from the CGLN amplitudes in the resonance maximum. The CGLN data have been taken from [22]. The quantities $I_{\text{GDH}}(\text{proton})$ and $I_{\text{GDH}}(\text{neutron})$ are the contributions of the respective resonance to the GDH integral. Lines 15–17: Nonresonant contributions to the GDH integral. Line 19: Predictions of the Regge model for contributions to the GDH integral according to [20].

resonance	A_n	$A_n(\text{proton})$	$I_{\text{GDH}}(\text{proton})$ [μb]	$A_n(\text{neutron})$	$I_{\text{GDH}}(\text{neutron})$ [μb]
$P_{33}(1232)$	$+1$	$+1.26$	$+291 \pm 15$	$+1.26$	$+291 \pm 15$
$P_{11}(1440)$	-2	-2.0	-11.6 ± 2.7	-2.0	-4.4 ± 2.3
$D_{13}(1520)$	$+1$	$+1.91$	$+77.5 \pm 7.8$	$+1.23$	$+40.2 \pm 6.5$
$S_{11}(1535)$	-2	-2.0	-22.6 ± 9.0	-2.0	-6.1 ± 3.5
$S_{11}(1650)$	-2	-2.0	-6.4 ± 1.9	-2.0	-0.5 ± 0.5
$D_{15}(1675)$	$+2/3$	$+0.67$	$+0.4 \pm 0.4$	$+0.67$	$+4.2 \pm 2.1$
$F_{15}(1680)$	$+2/3$	$+1.88$	$+35.0 \pm 3.5$	$+0.76$	$+1.5 \pm 0.6$
$D_{33}(1700)$	$+1$	±0.0	0.0 ± 3.5	±0.0	0.0 ± 3.5
$F_{35}(1905)$	$+2/3$	$+1.31$	$+2.8 \pm 1.6$	$+1.31$	$+2.8 \pm 1.6$
$P_{33}(1920)$	$+1$	$+1.0$	$+1.7 \pm 1.2$	$+1.0$	$+1.7 \pm 1.2$
$F_{37}(1950)$	$+1/2$	$+0.56$	$+5.6 \pm 1.7$	$+0.56$	$+5.6 \pm 1.7$
	resonant	sum	374 ± 20		336 ± 18
nonres(E_{0+})			-147		-184
nonres($(M,E)_{1+}^{(1/2)}$)			$+13$		$+47$
nonres($M_{1-}^{(3/2)}$)			-9		-9
	present	total	231 ± 20		190 ± 18
final result	Regge	predicted	-15		$+41$
	Regge	included	216 ± 20		231 ± 18
		sum rule	205		233

There have been many arguments accumulated over the years that $g(\infty) = 0$ (see e.g. [20]). Assuming that this no-subtraction hypothesis is fulfilled we arrive at the frequently cited GDH sum rule

$$\int_{\omega_0}^{\infty} \frac{d\omega}{\omega} \left[\sigma_{3/2}(\omega) - \sigma_{1/2}(\omega) \right] = 2\pi^2 \alpha_e \left(\frac{\kappa}{m} \right)^2 . \tag{54}$$

By combining Eqs. (51) and (54) the GDH dispersion relation may be written in the form

$$\operatorname{Re} g_0(\omega) = \omega \operatorname{Re} g(\omega) = \frac{\omega}{4\pi^2} \mathcal{P} \int_{\omega_0}^{\infty} \frac{\omega' \, \Delta\sigma(\omega')}{\omega'^2 - \omega^2} d\omega'. \tag{55}$$

For comparison see e.g. [5, 20, 46].

4.1 Contributions of resonant and nonresonant excitation processes to the GDH integral

Explicit expressions for the helicity and isospin dependent cross sections are given in Eqs. (11) to (24). For the E_{0+} multipole both isospin components make a contribution to the nonresonant cross section and up to 500 MeV this cross section is purely nonresonant. Resonant contributions from the E_{0+} multipole show up at higher energies in the $S_{11}(1535)$, the $S_{31}(1620)$ and the $S_{11}(1650)$ resonances. Therefore, in order to obtain the nonresonant E_{0+} cross section above 500 MeV we have to make an extrapolation. This is possible with sufficient precision by adjusting the Born approximation to the experimental data.

For the M_{1-} multipole the $I = 3/2$ component makes a contribution to the nonresonant cross section whereas the $I = 1/2$ component is exhausted by the $P_{11}(1440)$ resonance. For the M_{1+} and E_{1+} multipoles the $I = 1/2$ component makes a contribution to the nonresonant cross section whereas the $I = 3/2$ component is exhausted by the $P_{33}(1232)$ resonance. For the nonresonant cross sections we make explicit use of the expressions given in Eqs. (11) to (16). This implies that we take into account the 1π channel only. This certainly is correct at low energies where the main contributions to the GDH integral are located.

For the resonant contributions we make use of the expression in Eq. (25) which relates the difference of the helicity dependent cross sections to the total photo-absorption cross section. The advantage of this procedure is that use can be made of the Walker parameterization of the total photo-absorption cross section and of the predictions for the peak cross sections obtained from the resonance couplings (see Eqs. (27) to (42)). Through this procedure the 2π and η photoproduction channels are implicitly taken into account. The proportionality constants A_n can be easily determined in case there is only one multipole either electric $E_{l\pm}$ or magnetic $M_{\pm}$. This is shown in column 2 of Table 3. In case of multipolarity mixing strong deviations from the quantities A_n given in column 2 of Table 3 are observed. In this case the quantities A_n can be predicted by evaluating the appropriate expression as given in (11) to (24) at the resonance peak using CGLN amplitudes [22]. The result of this procedure is given in columns 3 and 5 of Table 3. It is interesting to note that the 2π decay component of the $D_{13}(1520)$ has been experimentally observed in the reactions $\vec{\gamma}\vec{p} \to n\pi^+\pi^0$ and $\vec{\gamma}\vec{p} \to p\pi^0\pi^0$ [10, 16]. These decay components are taken care of in the present analysis by using the total cross section of the $D_{13}(1520)$ resonance with the 2π decay component included.

Another nonresonant contribution is expected at high energies from diffractive effects and can be calculated using Regge parameterizations. Estimates carried out in [20] yields $I_{\text{GDH}}^{\text{Regge}}(\text{proton}) = -15\mu\text{b}$ and $I_{\text{GDH}}^{\text{Regge}}(\text{neutron}) = +41\mu\text{b}$. Including these diffractive (Regge) contributions into the calculation we arrive at the final results $I_{\text{GDH}}(\text{proton}) = (216 \pm 20)\mu\text{b}$ and $I_{\text{GDH}}(\text{neutron}) =$

Table 4: Non-Regge contributions to the GDH integral. The data of Workman and Arndt, Sandorfi et al. and Drechsel and Krein contain the two-pion correction calculated by Karliner. The data of Fix and Arenhövel and of the present work contain two-pion corrections developed in the respective works.

	$I_{\mathrm{GDH}}^{\mathrm{p}}$	$I_{\mathrm{GDH}}^{\mathrm{n}}$
Karliner [25]	261	183
Workman, Arndt [47]	260	192
Sandorfi et al. [48]	289	160
Drechsel, Krein [49]	261	180
Fix, Arenhövel [50]	216.58	190.51
present work	231 ± 20	190 ± 18
experiment [13, 19, 20]	226 ± 13	214 ± 35

$(231 \pm 18)\mu$b. It is of interest to compare the present approach to the GDH sum rule with previous approaches. This is carried out in Table 4. There is a general satisfactory agreement between the different predictions. Experimental data on helicity dependent photo-absorption cross sections have been measured at MAMI (Mainz) and ELSA (Bonn) [6–19]. The experimental data for the proton given in Table 4 have been taken from

$$I_{\mathrm{run}}^{^{1}H}(2.9 \text{ GeV}) = 226 \pm 5_{\mathrm{stat}} \pm 12_{\mathrm{syst}} \ \mu\text{b} \tag{56}$$

as given in [13, 20]. The experimental data for neutron have been taken from

$$I_{\mathrm{run}}^{^{2}H}(1.8 \text{ GeV}) = 440 \pm 21_{\mathrm{stat}} \pm 25_{\mathrm{syst}} \ \mu\text{b} \tag{57}$$

as given in [19] by subtracting the value for the proton as given in (56). Comparing the different predictions with the experimental data, it appears that the results of the present work are in closest agreement.

4.2 Predicted difference of helicity dependent cross sections compared with experimental data

Recent measurements at MAMI (Mainz) and ELSA (Bonn) have led to very valuable data for the helicity dependence of the total photo-absorption cross section of the proton and the neutron. In the following we will compare experimental data obtained for the proton with the predictions of the present approach. We restrict the discussion to the proton because of the higher precision of the experimental data as compared to the neutron.

In Figure 1 we discuss experimental data obtained at MAMI (Mainz). In order to clearly demonstrate the resonant structure of the first and the second resonance we have eliminated the nonresonant contribution from the figure and only keep the resonant contribution. The baseline of the resonant contribution now is the abscissa. Technically this has been achieved by adding the predicted nonresonant contribution to the experimental data. The $P_{33}(1232)$ and $D_{13}(1520)$ make strong positive contributions whereas the $P_{11}(1440)$ and the $S_{13}(1535)$ make small negative contributions. During the fitting procedure it was found out that slight shifts of some of the parameters within their margins of errors led to an improvement of the fit to the experimental data. For the $P_{33}(1232)$ resonance these shifts are 1232 MeV $\rightarrow$ 1226 MeV for the position of the peak, 130 MeV $\rightarrow$ 120 MeV for the width of the resonance and 1.26 $\rightarrow$
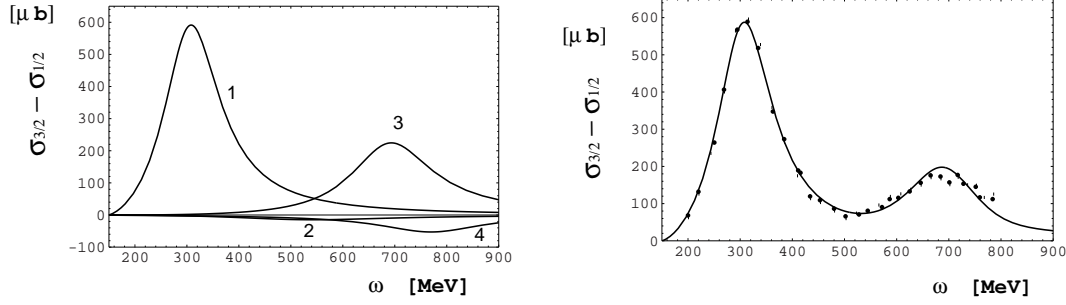
Figure 1: Predicted difference of helicity dependent cross sections for the proton in the first and second resonance region compared with experimental data. The experimental data are taken from [7]. The nonresonant contribution is eliminated from the figure by a procedure described in the text. The contributions shown in the left panel are the resonances $P_{33}(1232)$ (1), $P_{11}(1440)$ (2), $D_{13}(1520)$ (3), and $S_{11}(1535)$ (4).
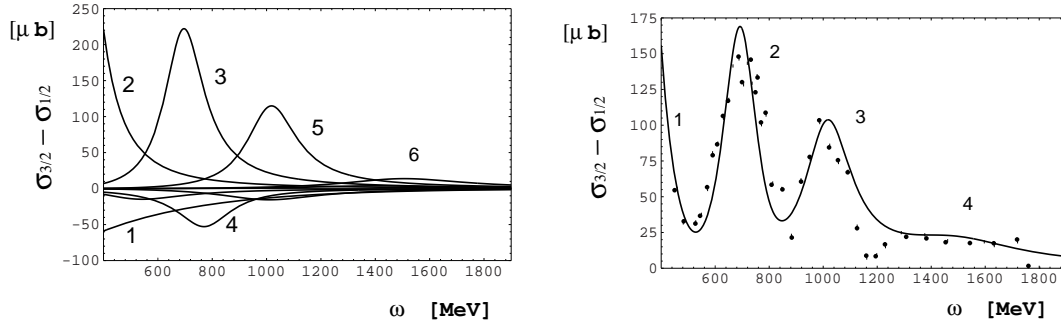

Figure 2: Predicted difference of helicity dependent cross sections for the proton in the second, third and fourth resonance region compared with experimental data. The experimental data are taken from [12]. The contributions shown in the left panel are the tail of the $P_{33}(1232)$ resonance (2), the nonresonant contribution (1), the $P_{11}(1440)$, $D_{13}(1520)$ (3), $S_{11}(1535)$ (4), $S_{11}(1650)$, $D_{15}(1675)$, $F_{15}(1680)$ (5), $D_{33}(1700)$, $F_{35}(1905)$ and $F_{37}(1950)$ (6) resonances. The numbers given in the right panel denote the resonance regions 1–4.

1.36 for the quantity A_n defined in Eq. (25). This means that the integrated cross section and also the integrated energy-weighted cross section remain constant. For the $D_{13}(1520)$ resonance the shifts were $1520 \rightarrow 1490$ for the position of the peak, 120 MeV $\rightarrow 130$ for the width of the resonance. All other parameters remained unmodified compared to the predictions given in Table 3.

Figure 2 differs from Figure 1 by the fact that the nonresonant contribution is not eliminated from the figure but included into the theoretical curve. Indeed, the dip between the first and the second resonance shown in the right panel of Figure 2 is strongly influenced by the nonresonant cross sections represented by curve 1 in the left panel. In the left panel only the stronger resonances have been identified through a number, though all the relevant resonances have been shown. As in Figure 1 some shifts of parameters have been tested in order to possibly improve on the fit to the experimental data. The only shift of some relevance was the generation of a small negative contribution from the $D_{33}(1700)$ by shifting the quantity A_n from $0 \rightarrow -0.5$.

The importance of the findings made in Figures 1 and 2 is that our procedure of applying the Walker parameterization to the helicity dependent cross section difference $(\sigma_{3/2} - \sigma_{1/2})$ has been

tested and found valid. This makes it possible to apply this procedure also to other problems as there is the prediction and interpretation of the s-channel contribution to the backward-angle spin-polarizability γ_π. Furthermore, we have clearly demonstrated that the upper part of the cross section in the right panel of Figure 2 is due to the $F_{37}(1950)$ resonance as anticipated before [12].

5 Polarizabilities

The appropriate tool for the prediction of electromagnetic polarizabilities is to simultaneously apply the forward-angle sum rule for $(\alpha + \beta)$ and the backward-angle sum rule for $(\alpha - \beta)$. This leads to the following relations [2] :

$$\alpha = \alpha^s + \alpha^t, \tag{58}$$

$$\alpha^s = \frac{1}{2\pi^2} \int_{\omega_0}^\infty [A(\omega)\sigma(\omega, E1, M2, \cdots) + B(\omega)\sigma(\omega, M1, E2, \cdots)] \frac{d\omega}{\omega^2}, \tag{59}$$

$$\alpha^t = \frac{1}{2}(\alpha - \beta)^t \tag{60}$$

and

$$\beta = \beta^s + \beta^t, \tag{61}$$

$$\beta^s = \frac{1}{2\pi^2} \int_{\omega_0}^\infty [A(\omega)\sigma(\omega, M1, E2, \cdots) + B(\omega)\sigma(\omega, E1, M2, \cdots)] \frac{d\omega}{\omega^2}, \tag{62}$$

$$\beta^t = -\frac{1}{2}(\alpha - \beta)^t, \tag{63}$$

with

$$\omega_0 = m_\pi + \frac{m_\pi^2}{2m}, \tag{64}$$

$$A(\omega) = \frac{1}{2}\left(1 + \sqrt{1 + \frac{2\omega}{m}}\right), \tag{65}$$

$$B(\omega) = \frac{1}{2}\left(1 - \sqrt{1 + \frac{2\omega}{m}}\right), \tag{66}$$

$$(\alpha - \beta)^t = \frac{g_{\sigma NN}\mathcal{M}(\sigma \to \gamma\gamma)}{2\pi m_\sigma^2} + \frac{g_{f_0 NN}\mathcal{M}(f_0 \to \gamma\gamma)}{2\pi m_{f_0}^2} + \frac{g_{a_0 NN}\mathcal{M}(a_0 \to \gamma\gamma)}{2\pi m_{a_0}^2}\tau_3. \tag{67}$$

In (58) to (67) ω is the photon energy in the lab. system, m_π the pion mass and m the nucleon mass. The quantities α^s, β^s are the s-channel electric and magnetic polarizabilities, and α^t, β^t the t-channel electric and magnetic polarizabilities, respectively. The multipole content of the photo-absorption cross-section enters through

$$\sigma(\omega, E1, M2, \cdots) = \sigma(\omega, E1) + \sigma(\omega, M2) + \cdots, \tag{68}$$

$$\sigma(\omega, M1, E2, \cdots) = \sigma(\omega, M1) + \sigma(\omega, E2) + \cdots, \tag{69}$$

i.e. through the sums of cross-sections with change and without change of parity during the electromagnetic transition, respectively. The multipoles belonging to parity change are favored for the electric polarizability α^s whereas the multipoles belonging to parity nonchange are favored for the magnetic polarizability β^s. For the t-channel parts we use the pole representations described in [3].

The backward spin-polarizability is given by [3, 51]

$$\gamma_\pi = \int_{\omega_0}^\infty \sqrt{1 + \frac{2\omega}{m}} \left(1 + \frac{\omega}{m}\right) \times \sum_n P_n [\sigma_{3/2}^n(\omega) - \sigma_{1/2}^n(\omega)] \frac{d\omega}{4\pi^2 \omega^3} + \gamma_\pi^t, \tag{70}$$

$$\gamma_\pi^t = \frac{1}{2\pi m} \left[\frac{g_{\pi NN} \mathcal{M}(\pi^0 \to \gamma\gamma)}{m_{\pi^0}^2} \tau_3 + \frac{g_{\eta NN} \mathcal{M}(\eta \to \gamma\gamma)}{m_\eta^2} + \frac{g_{\eta' NN} \mathcal{M}(\eta' \to \gamma\gamma)}{m_{\eta'}^2} \right]. \tag{71}$$

where the parity factor is $P_n(E1, M2, \cdots) = -1$ and $P_n(M1, E2, \cdots) = +1$. The quantities g_{MNN} are the meson-nucleon coupling constants and $\mathcal{M}(M \to \gamma\gamma)$ the decay matrix elements.

5.1 The t-channel contributions of the polarizabilities

As stated before a very large part of the polarizabilities is not due to excitations of the quark-structure of the nucleon but due to the coupling of the constituent quarks to scalar and pseudoscalar mesons being capable of a two-photon decay. The π^0 meson pole has been proposed in 1958 [52], the scalar-isoscalar t-channel in 1962 [53]. In several papers it has been attempted to construct $(\alpha - \beta)^t$ from the reactions $\gamma\gamma \to \pi\pi$ and $\pi\pi \to N\bar{N}$ (see [5] for a summary). This latter approach has been reconsidered very recently [54] in an attempt to derive the two-photon width of the σ meson from the experimental $(\alpha - \beta)^t$.

The first attempts to calculate $(\alpha - \beta)^t$ from a σ–pole ansatz has been made in [5, 45] and presented in its final form in [1]. The basic idea of this approach is that scalar and pseudoscalar mesons showing up as t-channel exchanges correspond to poles located in the unphysical region of the s-t plane and, therefore, may have properties different from those of the corresponding on-shell particles, except for their two-photon widths $\Gamma_{\gamma\gamma}$. Furthermore, it may be allowed to represent the t-channel exchanges in terms of a $q\bar{q}$ core of the meson. For the σ meson this approach follows the theory of Delbourgo and Scadron [55] which treats chiral symmetry breaking in the dynamical linear σ model on the quark level. The application to the present problem is described in [1–4]. The results derived in [3] are listed in Table 6.

5.2 Numerical results

The numerical results obtained for the polarizabilities are shown in Tables 5 and 6. Table 5 shows the s-channel contributions of the polarizabilities. For the spin-polarizabilities of resonant states the scaling factor (26) depending on the multipolarity mixing has to be taken into account. This is important for the $P_{33}(1232)$ resonance where two options $viz.$ $A_n(P_{33}(1232)) = 1.26$ and $A_n(P_{33}(1232)) = 1.0$ are compared with each other. The corresponding results are given in lines 2 and 3 of Table 5. In Table 6 the t-channel contributions are added and a comparison of the results with experimental data is carried out. In addition to the present results also the predictions of L'vov and Nathan [51] are shown.

Some remarks have to be made concerning the contribution labeled $\gamma N \to \pi\Delta$. This contribution contains all reactions with more than one pion in the final state where the $\gamma N \to \pi\Delta$ contribution is the most prominent one, except for those where the nucleon resonant states are the intermediate states. For the spin polarizabilities the predictions are taken from [51]. For the electric and magnetic polarizabilities the multipolarity ratio $E1/M1$ has to be known which was adopted to be $70\%(E1)$ and $30\%(M1)$ for sake of consistency of the prediction with the

15

Table 5: Resonant (lines 2–13) and single-pion nonresonant (lines 16–18) components of the polarizabilities. The electric and magnetic polarizabilities are in unite of 10^{-4}fm^3, the spin polarizabilities in unite of 10^{-4}fm^4. (a) Present predictions with $A_n(P_{33}(1232)) = 1.26$ (see (26)), (b) with $A_n(P_{33}(1232)) = 1.0$. res.+1π-nr: resonant +1π nonresonant contribution.

	α_p	β_p	α_n	β_n	$\gamma_\pi^{(p)}$	$\gamma_\pi^{(n)}$
$P_{33}(1232)$	-1.07	$+8.32$	-1.07	$+8.32$	$+5.11$(a)	$+5.11$(a)
					$+4.05$(b)	$+4.05$(b)
$P_{11}(1440)$	-0.02	$+0.14$	-0.01	$+0.05$	-0.10	-0.04
$D_{13}(1520)$	$+0.68$	-0.16	$+0.55$	-0.13	-0.39	-0.20
$S_{11}(1535)$	$+0.21$	-0.05	$+0.06$	-0.01	$+0.13$	$+0.04$
$S_{11}(1650)$	$+0.05$	-0.01	$+0.00$	-0.00	$+0.03$	$+0.00$
$D_{15}(1675)$	$+0.01$	-0.00	$+0.08$	-0.02	-0.00	-0.01
$F_{15}(1680)$	-0.07	$+0.25$	-0.01	$+0.03$	$+0.13$	$+0.01$
$D_{33}(1700)$	$+0.25$	-0.07	$+0.25$	-0.07	-0.00	-0.00
$F_{35}(1905)$	-0.01	$+0.02$	-0.01	$+0.02$	$+0.01$	$+0.01$
$P_{33}(1920)$	-0.01	$+0.02$	-0.01	$+0.02$	$+0.01$	$+0.01$
$F_{37}(1950)$	-0.03	$+0.10$	-0.03	$+0.10$	$+0.01$	$+0.01$
sum-res	-0.01	$+8.56$	-0.20	$+8.31$	$+4.94$(a)	$+4.94$(a)
					$+3.88$(b)	$+3.88$(b)
E_{0+}	$+3.19$	-0.34	$+4.07$	-0.43	$+3.75$	$+4.81$
$M_{1-}^{(3/2)}$	-0.04	$+0.35$	-0.04	$+0.35$	-0.18	-0.18
$(M,E)_{1+}^{(1/2)}$	-0.06	$+0.47$	-0.21	$+1.44$	$+0.24$	$+0.66$
res.+1π-nr	$+3.08$	$+9.04$	$+3.62$	$+9.67$	$+8.75$(a)	$+10.23$(a)
					$+7.69$(b)	$+9.17$(b)

experimental data. At present there is no easy possibility to determine the multipolarity ratio $E1/M1$ from theoretical arguments only.

For the s-channel parts of the spin-polarizabilities four different predictions are compared with each other in lines 2 – 5 of Table 6. We notice that the present results (a) are in better agreement with the L'vov result [51] (d) and the present results (b) with the L'vov [51] results (c). The deviations of the predictions (a) – (d) in lines 10 –13 from the experimental results are smaller than the experimental errors. Therefore, improvements may be expected from higher precision of the experimental data in the first place.

6   Discussion

In the present investigation we have shown that the level scheme of the nucleon corresponding to the first three oscillator shells of the $SU(6)$-HO model is well understood. As a specific feature we have found that for I=1/2 the photo-excitation strengths of resonant states in the neutron are smaller than the corresponding quantities of the proton. An explanation for this specific feature is provided by the quark model where this feature shows up as a consequence of the different electric charges of the quarks entering into electromagnetic transition matrix elements. One consequence of this feature is that the radiative width of the $F_{15}(1680)$ resonance is only exceptionally large in the proton but rather small in the neutron. Therefore, for the neutron the third resonance region showing up in the photoexcitation spectrum is not dominated by the

Table 6: Lines 2–5: Resonant + 1π nonresonant components of polarizabilities. (a) Present prediction with $A_n(P_{33}(1232)) = 1.26$, (b) with $A_n(P_{33}(1232)) = 1.0$, (c) L'vov [51] based on the SAID parameterization of CGLN amplitudes (d) L'vov [51] based on the HDT parameterization of CGLN amplitude. Lines 6–8: Scalar and pseudoscalar t-channel components as derived in [3]. Line 9: Nonresonant 2π channel with $\gamma N \to \pi\Delta$ as the main component. Lines 10–13: Total predicted polarizabilities. Lines 14–15: The experimental results labeled "exp." are those of the analysis in Ref. [5], the experimental results labeled "exp. corr" are those of the analysis in Ref. [3].

	α_p	β_p	α_n	β_n	$\gamma_\pi^{(p)}$	$\gamma_\pi^{(n)}$
res.+1π nr	+3.08	+9.04	+3.62	+9.67	+8.75(a)	+10.23(a)
					+7.69(b)	+9.17(b)
					+7.31(c)	+9.35(c)
					+8.37(d)	+9.76(d)
σ/π^0-t-ch.	+7.6	−7.6	+7.6	−7.6	−46.7	+46.7
f_0/η-t-ch.	+0.3	−0.3	+0.3	−0.3	+1.2	+1.2
a_0/η'-t-ch.	−0.4	+0.4	+0.4	−0.4	+0.4	+0.4
$\gamma N \to \pi\Delta$	+1.4	+0.4	+1.5	+0.4	−0.28	−0.23
sum	12.0	+1.9	+13.4	+1.8	−36.6(a)	+58.3(a)
					−37.7(b)	+57.2(b)
					−38.1(c)	+57.4(c)
					−37.0(d)	+57.8(d)
exp.	+12.0 ± 0.6	+1.9 ∓ 0.6	+12.5 ± 1.7	+2.7 ∓ 1.8	−38.7 ± 1.8	58.6 ± 4.0
exp. corr.	+12.0 ± 0.6	+1.9 ∓ 0.6	+13.4 ± 1.0	+1.8 ∓ 1.0	−38.7 ± 1.8	57.6 ± 1.8

$F_{15}(1680)$ resonance but by the $D_{33}(1700)$ resonance. An exception of this general intensity rule is only observed for the $D_{15}(1675)$ resonance where the Moorhouse [32] selection rule predicts a very small photoexcitation strength for the proton.

A further success of the present approach is the quantitative representation of helicity dependent cross section $(\sigma_{3/2} - \sigma_{1/2})$ in terms of resonant and nonresonant contributions and the good agreement of the predictions with experimental data. An interesting result obtained in this connection is that the resonant structure of the $(\sigma_{3/2} - \sigma_{1/2})$ cross section is much more dependent on the mixture of multipoles than the resonant structure of the total cross section σ_T. For the $P_{33}(1232)$ resonance the E_{1+} component enhances the partial $(\sigma_{3/2} - \sigma_{1/2})$ cross section by 26%. The experimental spectra shown in Figures 1 and 2 are well understood. Especially the peak structure in Figure 2 around 1500 MeV can clearly be interpreted in terms of the $F_{37}(1950)$ resonance.

For the polarizabilities α, β and γ_π the $P_{33}(1232)$ resonance dominates the resonant s-channel contribution and the electric-dipole "pion-cloud" amplitude E_{0+} the nonresonant s-channel contribution. In addition the σ-meson t-channel exchange makes a large contribution to the electric (α) and magnetic (β) polarizabilities. For the electric polarizability the σ-meson t-channel contribution is about twice as large as the "pion-cloud" E_{0+} contribution. For the magnetic polarizability the σ-meson t-channel contribution explains the pronounced diamagnetism of the nucleon. For the backward spin-polarizability the π^0 t-channel contribution is larger than the s-channel contributions by a factor of ≈ 5.

It should be noted that a comparison between results from chiral perturbation theory and dispersion theory has been carried out in [2].

Appendix

A   Level scheme of the nucleon

Figure A1 shows the level scheme of the nucleon corresponding to the first three HO shells. In total four resonance regions are formed. The first resonance region is solely due to the
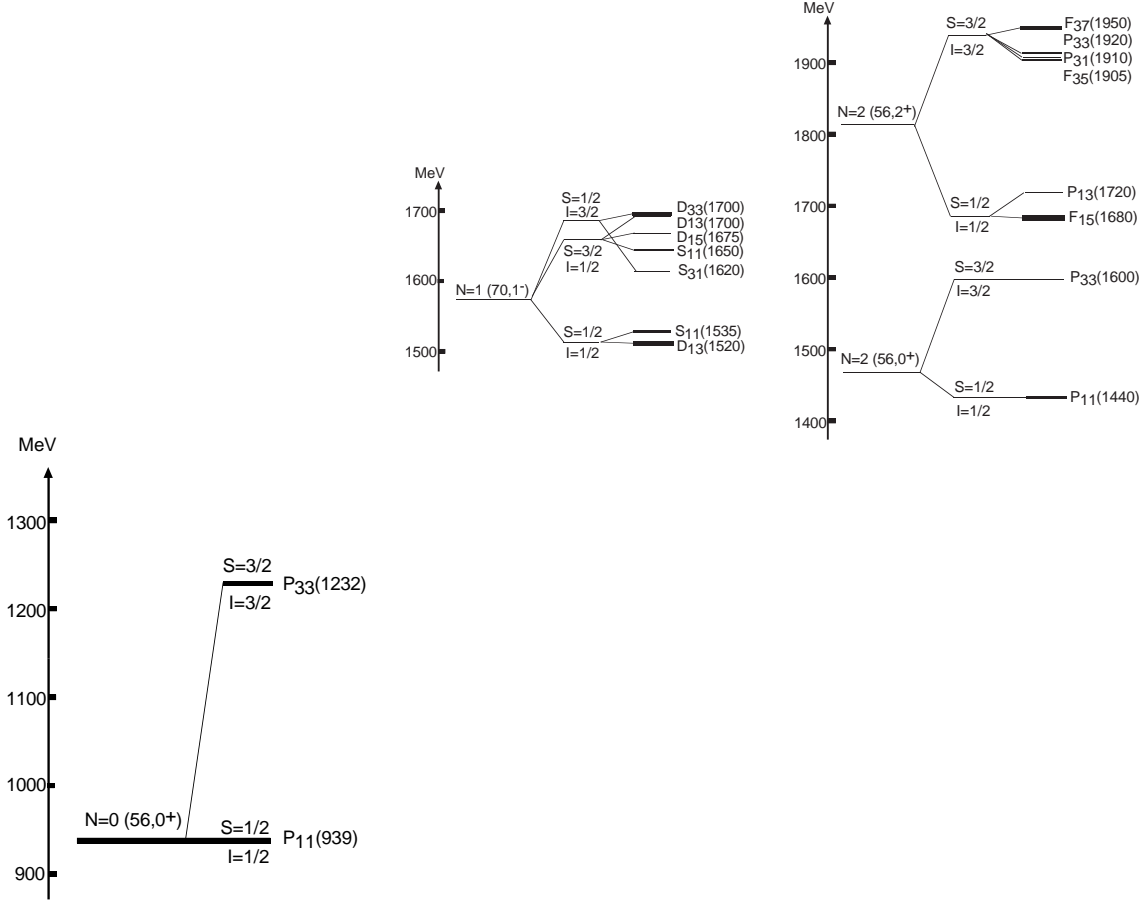
MeV

S=3/2   F$_{37}$(1950)
I=3/2   P$_{33}$(1920)
P$_{31}$(1910)
F$_{35}$(1905)

1900

N=2 (56,2$^+$)

1800

MeV

S=1/2   P$_{13}$(1720)
I=1/2   F$_{15}$(1680)

MeV

1700   S=1/2   D$_{33}$(1700)
I=3/2   D$_{13}$(1700)
D$_{15}$(1675)
S$_{11}$(1650)
S=3/2   S$_{31}$(1620)
I=1/2

1700

1600   N=1 (70,1$^-$)

S=3/2   P$_{33}$(1600)
I=3/2

1600

1500   S=1/2   S$_{11}$(1535)
I=1/2   D$_{13}$(1520)

1500   N=2 (56,0$^+$)

S=1/2   P$_{11}$(1440)
I=1/2

1400

MeV

1300

S=3/2   P$_{33}$(1232)

1200   I=3/2

1100

1000

N=0 (56,0$^+$)   S=1/2   P$_{11}$(939)
I=1/2

900

Figure A1: The $N = 0$ $(56,0^+)$ (left), $N = 1$ $(70,1^-)$ (middle), and $N = 2$ $(56,0^+)$, $(56,2^+)$ (right) partial level schemes of the nucleon

$P_{33}(1232)$ state which as a $I = 3/2$ state is of equal photon-excitation strength in the proton and the neutron. The second resonance region is due to the $D_{13}(1520)$ and the $S_{11}(1535)$ states. As $I = 1/2$ states the strength is larger in the proton than in the neutron in both resonances. The third resonance region consists of the $F_{15}(1680)$ and the $D_{33}(1700)$ states. For the proton the two contributions are of approximately equal strength, whereas for the neutron according to the general rule for $I = 1/2$ states the $F_{15}(1680)$ contribution is largely suppressed. The fourth resonance is due to the $F_{37}(1950)$ state which is of equal strength in the proton and the neutron.

B   Resonance parameters of the nucleon

Table B1: Resonance parameters of proton resonant states for the first three oscillator shells. The sixth column denoted by $I_{int.}(p)$ contains the integrated photo-absorption cross sections for the proton as following from the data given in columns 2–5. The ordering of levels is the same as in Table 1.

	$10^3\,A_{1/2}$ [GeV$^{-1/2}$]	$10^3\,A_{3/2}$ [GeV$^{-1/2}$]	Γ_r [MeV]	I_r [μb]	$I_{int.}(p)$ [$10^3\,\mu$b MeV]
$P_{33}(1232)$	-139 ± 3	-257 ± 4	130 ± 5	390 ± 10	80.0 ± 4.0
$P_{11}(1440)$	-65 ± 4	–	350 ± 70	6.1 ± 1.4	3.4 ± 0.8
$P_{33}(1600)$	-23 ± 20	-9 ± 21	330 ± 50	0.8 ± 0.8	0.7 ± 0.6
$S_{11}(1535)$	$+90 \pm 20$	–	150 ± 30	26 ± 10	8.8 ± 3.5
$D_{13}(1520)$	-24 ± 9	$+166 \pm 5$	120 ± 10	113 ± 11	34.6 ± 3.5
$S_{31}(1620)$	$+27 \pm 11$	–	140 ± 20	2.4 ± 1.4	0.9 ± 0.5
$D_{33}(1700)$	$+104 \pm 15$	$+85 \pm 22$	270 ± 70	29 ± 12	18.0 ± 3.6
$S_{11}(1650)$	$+53 \pm 16$	–	160 ± 10	7.8 ± 2.3	3.1 ± 0.9
$D_{13}(1700)$	-18 ± 13	-2 ± 24	100 ± 20	1.4 ± 1.0	0.4 ± 0.3
$D_{15}(1675)$	$+19 \pm 8$	$+15 \pm 9$	150 ± 10	1.7 ± 1.0	0.7 ± 0.4
$P_{13}(1720)$	$+18 \pm 30$	-19 ± 20	150 ± 30	1.9 ± 1.9	0.8 ± 0.8
$F_{15}(1680)$	-15 ± 6	$+133 \pm 12$	130 ± 10	60 ± 12	19.9 ± 2.0
$P_{31}(1910)$	$+3 \pm 14$	–	240 ± 20	0.01 ± 0.01	< 0.1
$P_{33}(1920)$	$+40 \pm 14$	$+23 \pm 17$	200 ± 40	4.0 ± 2.5	2.3 ± 1.6
$F_{35}(1905)$	$+26 \pm 11$	-45 ± 20	300 ± 60	3.5 ± 3.0	2.7 ± 1.5
$F_{37}(1950)$	-76 ± 12	-97 ± 10	280 ± 20	20.3 ± 5.0	15.8 ± 4.0

Table B2: Resonance parameters of neutron resonant states for the first three oscillator shells. The sixth column denoted by $I_{int.}(\text{n})$ contains the integrated photo-absorption cross sections for the neutron as following from the data given in columns 2-5. The ordering of levels is the same as in Table 1.

	$10^3 A_{1/2}$ $[\text{GeV}^{-1/2}]$	$10^3 A_{3/2}$ $[\text{GeV}^{-1/2}]$	Γ_r $[\text{MeV}]$	I_r $[\mu\text{b}]$	$I_{int.}(\text{n})$ $[10^3 \, \mu\text{b MeV}]$
$P_{33}(1232)$	-139 ± 3	-257 ± 4	130 ± 5	390 ± 10	80.0 ± 4.0
$P_{11}(1440)$	$+40 \pm 10$	$-$	350 ± 70	2.3 ± 1.2	1.3 ± 0.7
$P_{33}(1600)$	-23 ± 20	-9 ± 21	330 ± 50	0.8 ± 0.8	0.7 ± 0.6
$S_{11}(1535)$	-46 ± 27	$-$	150 ± 30	7 ± 4	2.4 ± 1.4
$D_{13}(1520)$	-59 ± 9	-139 ± 11	120 ± 10	91 ± 15	27.9 ± 4.6
$S_{31}(1620)$	$+27 \pm 11$	$-$	140 ± 20	2.4 ± 1.4	0.9 ± 0.5
$D_{33}(1700)$	$+104 \pm 15$	$+85 \pm 22$	270 ± 70	29 ± 12	18.0 ± 3.6
$S_{11}(1650)$	-15 ± 21	$-$	160 ± 10	0.6 ± 0.6	0.2 ± 0.2
$D_{13}(1700)$	0 ± 50	-33 ± 44	100 ± 20	0.5 ± 0.5	0.1 ± 0.1
$D_{15}(1675)$	-43 ± 12	-58 ± 13	150 ± 10	15 ± 5	6.2 ± 2.1
$P_{13}(1720)$	$+1 \pm 15$	-29 ± 61	150 ± 30	2.3 ± 3.0	1.0 ± 1.0
$F_{15}(1680)$	$+29 \pm 10$	-33 ± 9	130 ± 10	6.5 ± 2.8	2.2 ± 0.9
$P_{31}(1910)$	$+3 \pm 14$	$-$	240 ± 20	0.01 ± 0.01	< 0.1
$P_{33}(1920)$	$+40 \pm 14$	$+23 \pm 17$	200 ± 40	4.0 ± 2.5	2.3 ± 1.6
$F_{35}(1905)$	$+26 \pm 11$	-45 ± 20	300 ± 60	3.5 ± 3.0	2.7 ± 1.5
$F_{37}(1950)$	-76 ± 12	-97 ± 10	280 ± 20	20.3 ± 5.0	15.8 ± 4.0

References

[1] M. Schumacher, Eur. Phys. J. A **30** (2006) 413, Eur. Phys. J. A **32** (2007) 121 (E) [hep-ph/0609040]; M.I. Levchuk, A.I. L'vov, A.I. Milstein, M. Schumacher, Proceedings of the Workshop on the Physics of Excited Nucleons, NSTAR 2005 (2005) 389 [hep-ph/0511193].

[2] M. Schumacher, Eur. Phys. J. A **31** (2007) 327 [arXiv:0704.0200 hep-ph].

[3] M. Schumacher, Eur. Phys. J. A **34** (2007) 293 [arXiv:0712.1417 hep-ph].

[4] M. Schumacher, AIP Conference Proceedings 1030 (Workshop on Scalar Mesons and Related Topics Honoring Michael Scadrons's 70th Birthday - SCADRON70) (2008) 129 [arXiv:0803.1074 hep-ph]; and supplement [arXiv:0805.2823 hep-ph].

[5] M. Schumacher, Progress in Particle and Nuclear Physics **55** (2005) 567 [hep-ph/0501167].

[6] GDH Collaboration, J. Ahrens et al., Phys. Rev. Lett. **84** (2000) 5950.

[7] GDH Collaboration, J. Ahrens et al., Phys. Rev. Lett. **87** (2001) 022003 [hep-ex/0105089].

[8] GDH Collaboration, J. Ahrens et al., Phys. Rev. Lett. **88** (2002) 232002 [hep-ex/0203006].

[9] GDH Collaboration, K. Helbing et al., Nucl. Phys. Proc. Suppl. **105** (2002) 113.

[10] GDH Collaboration, J. Ahrens et al., Phys. Lett. B **551** (2003) 49.

[11] GDH Collaboration, J. Ahrens et al., Eur. Phys. J. A **17** (2003) 241.

[12] GDH Collaboration, H. Dutz et al., Phys. Rev. Lett. **91** (2003) 192001.

[13] GDH Collaboration, H. Dutz et al., Phys. Rev. Lett. **93** (2004) 032003.

[14] GDH Collaboration, J. Ahrens et al., Eur. Phys. J. A **21** (2004) 323.

[15] GDH Collaboration, H. Dutz et al., Phys. Rev. Lett. **94** (2005) 162001.

[16] GDH Collaboration, J. Ahrens et al., Phys. Lett. B **624** (2005) 173.

[17] GDH Collaboration, J. Ahrens et al., Eur. Phys. J. A **26** (2005) 135.

[18] GDH Collaboration, J. Ahrens et al. Phys. Rev. C **74** (2006) 045204.

[19] GDH Collaboration, J. Ahrens et al., Phys. Rev. Lett. **97** (2006) 202303.

[20] K. Helbing, Prog. Part. Nucl. Phys. **57** (2006) 405.

[21] D. Drechsel, L. Tiator, Ann Rev. Nucl. Part. Sci. **54** (2004) 69 [nucl-th/0406059].

[22] D. Drechsel, S.S. Kamalov, L. Tiator, Eur. Phys. J. **34** (2007) 69 [nucl-th/0710.0306].

[23] M. Dugger, et al., Phys. Rev. C **76** (2007) 025211.

[24] R.L. Walker, Phys. Rev. **182** (1969) 1729.

[25] I. Karliner, Phys. Rev. D **7** (1973) 2717.

[26] D. Drechsel et al., Nucl. Phys. A **645** (1999) 145.

[27] T. Ericson, W. Weise, *Pions and Nuclei*, Int Ser. Monogr. Phys., Vol. **74** (Oxford Science Publications, 1988).

[28] D. Drechsel, S.S. Kamalov, G. Krein, L. Tiator, Phys. Rev. D **59** (1999) 094021.

[29] T.A. Armstrong et al., Nucl. Phys. B**41** (1972) 445.

[30] Particle Data Group: C. Amsler, Phys. Lett. **B557** (2008) 1.

[31] R.A. Arndt et al., Phys. Rev. C **42** (1990) 1864.

[32] R.G. Moorhouse, Phys. Rev. Lett. **16** (1966) 772.

[33] D. Faiman, A. W. Hendry, Phys. Rev. **173** (1968) 1720; Phys. Rev. **180** (1969) 1572.

[34] D.B. Lichtenberg, Phys. Rev. **178** (1969) 2197.

[35] L.A. Copley, G. Karl, E. Obryk, Nucl. Phys. B **13** (1969) 303.

[36] R.P. Feynman, M. Kislinger, F. Ravndal, Phys. Rev. D **3** (1971) 2706.

[37] F.E. Close, *An Introduction to Quarks and Partons* Academic Press (London) 1979.

[38] R. Koniuk, N. Isgur, Phys. Rev. D **21** (1980) 1868.

[39] S. Capstick, N. Isgur, Phys. Rev. D **34** (1986) 2809.

[40] D.M. Manley, *Research Program at CEBAF (II), Report of the 1986 Summer Study Group* (1987) 199.

[41] F.E. Close, Z. Li, Phys. Rev. D **42** (1990) 2194.

[42] M. M. Giannini, Rep. Prog. Phys. **54** (1990) 453.

[43] S. Capstick, Phys. Rev. D **46** (1992) 2864.

[44] D.Y. Chen, Y.B. Dong, M.M. Giannini, E. Santopinto, Nucl. Phys. A **782** (2007) 62 [arXiv:nucl-th/0611016].

[45] A.I. L'vov, V.A. Petrun'kin, M. Schumacher, Phys. Rev. C **55** (1997) 359.

[46] D. Drechsel, B. Pasquini, M. Vanderhaeghen, Phys. Rept. **378** (2003) 99 [hep-ph/0212124].

[47] R.L. Workman, R.A. Arndt, Phys. Rev. D **45** (1992) 1789.

[48] A.M. Sandorfi, M. Khandaker, C.S. Whisnant, Phys. Rev. D **50** (1994) R6681.

[49] D. Drechsel, G. Krein, Phys. Rev. D **58** (1998) 116009 [hep-ph/9808230].

[50] A. Fix, H. Arenhövel, Eur. Phys. J. A **25** (2005) 115 [nucl-th/0503042].

[51] A.I. L'vov, A.M. Nathan, Phys. Rev. C **59** (1999) 1064.

[52] F.E. Low, *Proceedings of the 1958 Annual International Conference on High Energy Physics at CERN, p. 98*; F.E. Low, Phys. Rev. **120** (1960) 582 (and references therein); M. Jabob, J. Mathews, Phys. Rev. **117** (1960) 854.

[53] A.C. Hearn, E. Leader, Phys. Rev. **126** (1972) 789.

[54] J. Bernabeu, J. Prades, Phys. Rev. Lett. **100** (2008) 241804 [0802.1830 hep-ph]; J. Prades, J. Bernabeu, 14th High-Energy Physics International Conference in Quantum Chromodynamics, Montpellier, France 1–12 July 2008 [0809.2475 hep-ph].

[55] R. Delbourgo, M. Scadron, Mod. Phys. Lett. A **10** (1995) 251 [hep-ph/9910242]; Int. J. Mod. Phys. A **13** (1998) 657 [hep-ph/9807504]; M. Nagy, M.D. Scadron, G.E. Hite, Acta Phys. Slovaca **54** (2004) 427 [hep-ph/0406009].